Journal of Applied Polymer Science

Method for the synthesis of *para*-aramid nanofibers

Matthew P. Yeager, Christopher M. Hoffman, Jr., Zhiyong Xia, Morgana M. Trexler
Applied Physics Laboratory, Johns Hopkins University, Laurel, Maryland 20723
M.P.Y. and C.M.H. contributed equally to this article.
Correspondence to: M. M. Trexler (E-mail: morgana.trexler@jhuapl.edu)

ABSTRACT: The synthesis and electrospinning of novel *N*-substituted aramid nanofibers (ANFs) prepared from basic dispersions of commercial microscale Kevlar fibers are herein reported. The functionalized ANFs were characterized via Fourier transform infrared spectroscopy, ^{13}C solid-state nuclear magnetic resonance spectroscopy, and X-ray diffraction to confirm proper *N*-substitution of the side groups and to determine changes to the polymer crystallinity and stability. These analyses suggested that the electrospun ANFs consisted of numerous crystalline domains in the transverse fiber direction with large amorphous regions that were void of defects commonly found in commercial Kevlar fibers. A semi-empirical study of the variations in the solubility parameter due to various side chain moieties was conducted to facilitate solvent selection and to elucidate the enhanced solubility effects with selected organic solvents. These initial findings suggest a promising route for obtaining a new class of nanofibers with ultrahigh strength and stiffness.
 J. Appl. Polym. Sci. **2016**, *133*, 44082.

KEYWORDS: electrospinning; fibers; functionalization of polymers; polyamides; synthesis and processing

Received 4 April 2016; accepted 15 June 2016
DOI: 10.1002/app.44082

INTRODUCTION

The synthesis of one-dimensional (1D) nanostructures has garnered immense interest and research focus because of the broad range of unique and auspicious mechanical, electrical, and thermal properties achievable.[1–4] As previously hypothesized, Papkov and coworkers[5–7] recently demonstrated a remarkable enhancement in the tensile strength and toughness of electrospun fibers as a function of decreasing radii down to the nanoscale. These improvements were attributed to both the low nanofiber crystallinity, which resulted from rapid solvent evaporation, and a decrease in fiber defects as the diameter decreased.

Electrospinning is a popular method for producing nanoscale polymeric fibers with high uniformity; it has been successfully reported for virtually all known polymeric fibers in both melt form or from solution.[8,9] Kevlar [poly(*para*-phenylene terephthalamide) (PPTA)] fibers, on the other hand, have only been electrospun from concentrated sulfuric acid to yield nonuniform fibers that could not be produced on a large scale.[10] PPTA fibers demonstrate superior mechanical properties and chemical resistance because of enhanced interchain cohesion through extensive hydrogen-bonding interactions;[11–14] this is ideal for ballistic defense applications and high-rate load environments. Therefore, a scalable method for uniformly electrospinning PPTA nanofibers without sulfuric acid would be of significant interest.

Several methods have recently been used to enable the synthesis of nanoscale Kevlar fibers. The top-down dispersal of Kevlar via deprotonation in dimethyl sulfoxide (DMSO) yielded stable dispersions of aramid nanofibers (ANFs) with diameters ranging from of 3–30 nm and lengths upward of 10 μm.[15,16] The extraction of the fiber dispersions via repetitive layer-by-layer dip-coating methods yielded two-dimensional (2D) mats, but despite the promising in-plane and out-of-plane moduli of such layered ANF mats, isolation from DMSO and/or extrusion of the individual ANFs was not possible with this method because of limited solubility. It has been reported that pendant *N*-substitutions can enhance the solubility of PPTA in a variety of organic solvents[17–20]; however, these findings have not yet been applied to enable spinning or extrusion of nanoscale aramid fibers.

In this article, we report a scalable and practical method facilitated by side-chain substitutions that enhances polymer solubility in organic solvents for continuously electrospinning ANFs. A semi-empirical solubility study was conducted to corroborate the solubility effects. Electrospun ANFs were characterized via scanning electron microscopy (SEM) imaging, Fourier transform infrared (FTIR) spectroscopy, X-ray diffraction (XRD), and NMR analyses to confirm side-chain substitution and to determine the morphology and crystalline/amorphous domains of the resulting nanofibers.

Scheme 1. Overall reaction of the hydride-based method for achieving ANF dispersions. The addition of water to the highly basic DMSO solution was believed to complete the dispersal process due to hydroxyl anion formation.

EXPERIMENTAL

Materials

All of the PPTA fiber used was Kevlar KM2 yarn (850 denier) procured from DuPont USA. DMSO (99.9%, anhydrous), *N*,*N*-dimethylformamide (DMF; 99.8%, anhydrous), *N*,*N*-dimethylacetamide (DMAc; 99.8%, anhydrous), *N*-methyl-2-pyrrolidinone (NMP; 99.5%, anhydrous), sodium hydride (NaH; 95%, dry), potassium hydride (KH; 30%, dispersed in mineral oil), potassium hydroxide (KOH; 99.9%), 1-bromopropane (99%), 3-bromo-1-propene (99%), and 5-bromo-1-pentene (95%) were obtained from Sigma-Aldrich. Bromomethylbenzene (99%) and iodomethane (99%) were obtained from Alfa Aesar. PPTA and KH were cleaned before use, as described in their respective sections later. All other reagents were used without further purification.

Poly(*para*-phenylene terephthalate) Sizing Removal and Preparation

Before PPTA dispersal and functionalization, we removed protective fiber sizing and residual moisture from the fibers by first soaking the KM2 fibers in methanol for 12 h; we then vacuum-dried the fibers at 60 °C overnight.[21] Thermogravimetric analysis was conducted to confirm the removal of native moisture within the PPTA fibers.

Poly(*para*-phenylene terephthalate) Dispersion via KOH-, NaH-, or KH-Based Methods

Three different methods for PPTA dispersion were used over the course of this study: a KOH-based procedure that was originally reported by Yang *et al.*[15] and two novel hydride-based procedures. These different procedures enabled us to investigated the effects of various strength bases and, therefore, different dispersion times. Following the procedure reported by Yang *et al.*, we dissolved 3.0 g of PPTA fibers in 500 mL of DMSO with 3.0 g of KOH over the course of 7–10 days in a closed but atmospheric environment. The dark red solution was then decanted into a separate reaction flask to remove the excess KOH; this left a viscous dispersion of metalated ANFs.

Separate methods for PPTA dispersion were developed with alkali hydride reagents; this increased the speed of fiber dispersion at a cost of greater reaction complexity. With NaH under an inert environment, 1.0 g of NaH was added to 600 mL of DMSO, and the mixture was stirred for approximately 1 h until the solution cooled to room temperature. This reaction proceeded to form a DMSO solution of the highly basic reagent sodium methylsulfinylmethylide; after this, 2.0 g of dried PPTA fibers was added portion-wise over the course of 1 h with continuous stirring. The DMSO/sodium methylsulfinylmethylide/PPTA solution was stirred for 16 h, and then, the orange-colored solution was exposed to the atmosphere and stirred for another 1–2 h. During this stage, the complete dispersal of the PPTA fibers was achieved upon the absorption of atmospheric water to the basic solution, as evidenced by the formation of a dark red dispersion (Scheme 1).

Similar to what was done in the dispersion with NaH, 1.67 g of KH was first washed with hexanes and then added to 600 mL of DMSO under an inert environment to form a potassium methylsulfinylmethylide solution. Once cooled, 3.0 g of the dried PPTA fibers were added portion-wise to the basic solution and allowed to stir for 4 h until the solution turned opaque orange. The solution was then removed from the inert environment and stirred for an additional 2 h, at which time full dispersal was complete.

Preparation of the Electrospinning Solutions

Dissolved PPTA/DMSO solutions were each reacted with 4 equiv of alkyl electrophile (leaving group = Br or I) and stirred for 24 h. During this time, the solution color changed from dark red to transparent yellow; this was indicative of the nonresonance associated with the nucleophilic substitution at the amide nitrogen. There was also a substantial decrease in the viscosity (Scheme 2). This resulting solution was vacuum-distilled to dryness, then redissolved in about 20 mL of solvent (i.e., DMF, DMAc, and/or NMP), and dried via rotoevaporation. Redisperion in the same organic solvent and rotoevaporation was performed once more to ensure adequate DMSO removal. The dried product was redissolved once more to obtain the desired polymer solution concentration (20–50 wt %); this was

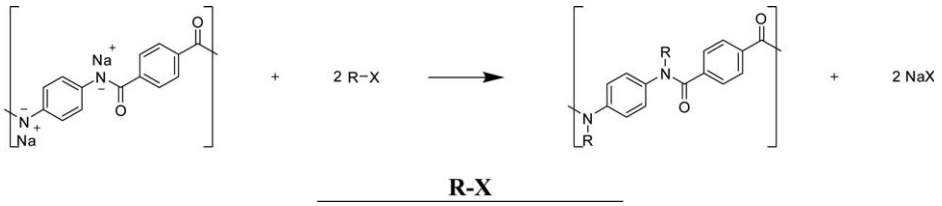

Scheme 2. *N*-functionalization step of the polyanionic aramid dispersion in DMSO with the alkyl electrophiles (R—X) used in this study.

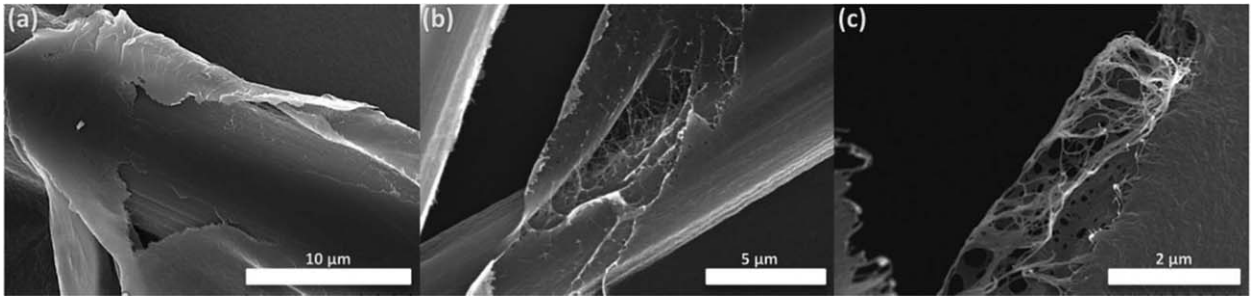

Figure 1. DMSO/KOH dispersal of Kevlar fibers after approximately (a) 50 and (b) 120 h. This illustrates the amorphous skin delamination from the inner core region of a single fiber. (c) Fully dispersed ANFs in a DMSO/KOH solution. The images were achieved via the drying of small aliquots of the respective ANF dispersals on 200-mesh copper transmission electron microscopy grids.

followed by sonication and centrifugation at 14,000g for 30 min to remove all excess salts.

Electrospinning Procedure and Conditions

Electrospinning was performed with a Bertan Series 230 power supply and a stationary aluminum foil target. The electrospinning solutions were pumped from a New Era NE-1000 syringe pump through a 22-gauge, blunt-tip stainless steel needle. The general electrospinning conditions used were solution concentrations from 20 to 50 wt %, a voltage of 20 kV, a volumetric flow rate of 0.1 mL/h, and a collector distance of 10 cm.

SEM

Fiber imaging and morphology characterization were performed with a Hitachi S4700 scanning electron microscope with a 2.0-kV accelerating voltage, an extraction current of 15 μA, and a working distance between 5.0 and 6.0 mm. All samples were iridium sputter-coated to an 8-nm thickness. Fiber diameter measurements were conducted with ImageJ software[22] with the associated DiameterJ plugin[23] with a fiber sample size of greater than 100 for each condition with five to eight randomly located images and captured at 18,000 × magnification.

^{13}C Solid-State Nuclear Magnetic Resonance (ssNMR)

^{13}C ssNMR was performed on electrospun ANFs to determine the structure and order of the aramid backbone and furthermore to properly confirm substitution at the amide site. ^{13}C ssNMR was conducted via cross-polarized magic angle spinning. The cross-polarized magic angle spinning data were obtained with a 1-ms mix time and a 3-s delay. Data were obtained on a Tecmag console-based spectrometer operating at an H-1 frequency of 363 MHz (C-13 at 91.4 MHz) and a spin speed of 4.8 kHz.

Elemental Analyses

Elemental analyses (via combustion product analyses) were conducted by Intertek Pharmaceutical Services to determine the relative CHNO elemental compositions of the ANFs after electrospinning.

FTIR Spectroscopy

FTIR spectroscopy was performed to confirm the presence of functional groups in the electrospun ANFs. All of the FTIR analyses were conducted in transmittance mode on a Bruker Vector 70 FTIR instrument via 128 individual scans between 400 and 4000 cm^{-1} at a resolution of 4 cm^{-1}. We prepared the FTIR samples by grinding approximately 1.0 g of functionalized ANFs with 300 g of potassium bromide (Sigma-Aldrich) and compressing the powder mixture for 15 min in a pellet press at 15,000 psi *in vacuo*. All of the electrospun ANF samples analyzed via FTIR spectroscopy were obtained from 20 wt % spinning solutions. The as-received KM2 samples were first cryomilled for six cycles (3-min duration each) with liquid nitrogen cooling to obtain a powder form for grinding purposes.

Table I. *N*-Functional Groups Used for Enhancing the ANF Solubility with the Solubility Parameter (δ) and Solvent Compatibility (Δδ) Values

Functional group name	Functional group structure	Calculated δ (MPa$^{1/2}$)[a]	Δδ (MPa$^{1/2}$)[b]		
			DMF	DMAc	NMP
None	—	26.0	1.2 (–)	3.3 (–)	3.1 (–)
Methyl		28.0	3.2 (–)	5.3 (–)	5.1 (+)
Propyl		22.8	2.0 (+)	0.1 (+)	0.1 (+)
Allyl		22.6	2.2 (+)	0.1 (+)	0.3 (+)
Pentenyl	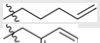	23.1	1.7 (+)	0.4 (+)	0.2 (+)
Benzyl		26.9	2.1 (–)	4.2 (+)	4.0 (+)
Hydroxypropyl		22.5	2.3 (–)	0.2 (–)	0.4 (–)

[a] The δ values of DMF, DMAc, and NMP were 24.8, 22.7, and 22.9 MPa$^{1/2}$, respectively.
[b] Δδ is the absolute difference between the solvent and ANF solubility parameters; + indicates solubility, and − indicates insolubility.

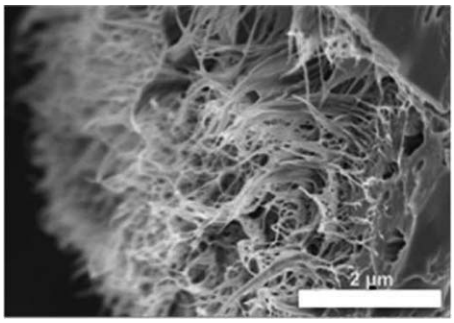

Figure 2. ANFs after functionalization with 1-bromopropane. They were redispersed in DMF and dried for comparison with unfunctionalized ANFs [Figure 1(b)] dried from a basic DMSO dispersion.

XRD

XRD data were obtained on a PaNalytical Empyrean Series 2 X-ray diffractometer with a Cu Kα light source (wavelength = 1.54056 Å, 1/4-in. divergent slit, 1/8-in. scatter slit) and collected by a 1D silicon strip detector over a 2θ range of 5–40° at 0.1° increments.

2D Small-Angle X-ray Scattering (SAXS)

2D SAXS was performed to probe and compare the lamellar structures of the electrospun ANFs and commercial Kevlar. All analyses were performed at the Brookhaven National Synchrotron Light Source on beamline X27C. The wavelength of the X-ray source was 1.371 Å. Before analyses, the sample-to-detector distance was calibrated with silver behenate to confirm a distance of 1817 mm. The samples were mounted on the sample stage with an incoming X-ray beam perpendicular to the sample plane. The 2D images were collected with a data-acquisition time of 100 s per image with a MarCCD 165 X-ray detector (Rayonix). All 2D images were recorded in transmission mode at room temperature and corrected for the main beam intensity fluctuation and sample absorption.

RESULTS AND DISCUSSION

Fiber Dispersion, Functionalization, and Solubility

Fibers at various stages were observed via SEM (Figure 1). The PPTA dispersion process [early stages shown in Figure 1(a,b)] resulted in fiber diameters on the order of 30 nm or less [Figure 1(c)]; this was consistent with previously reported observations.[15] The dispersion of the ANFs in DMSO was possible because the deprotonation of the polymer backbone amides disrupted the interfiber hydrogen-bonding network responsible for the backbone adhesion.[15] Multiple unsuccessful attempts were made to isolate these deprotonated nanofibers from the basic DMSO dispersion: (1) the removal of the DMSO solvent from the basic dispersion by vacuum distillation gave a brittle red solid that was insoluble in all other organic solvents, and (2) the addition of water or acid to DMSO caused the precipitation of completely insoluble PPTA, likely because the reintroduction of hydrogen bonding resulted in the immediate aggregation of ANFs into an unworkable mat. Alkylation of the deprotonated amide site of the ANF dispersion resulted in a rapid drop in solution viscosity with a concomitant color change to transparent yellow; this was indicative of functionalization.

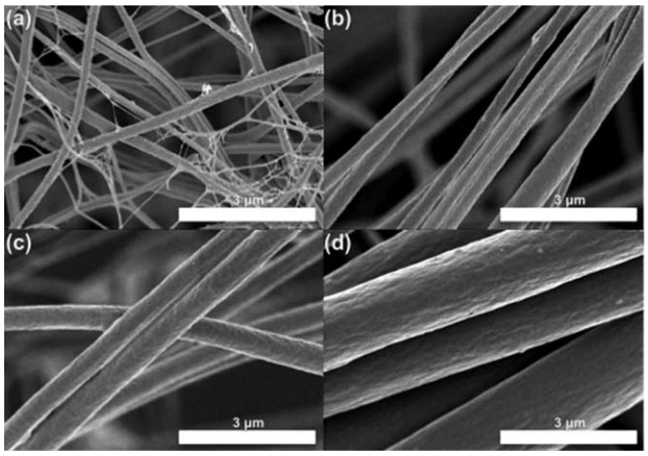

Figure 3. Propyl ANFs spun from DMF-based solutions with polymer concentrations of (a) 20, (b) 30, (c) 35, and (d) 50 wt %. The operating conditions were 20 kV, a 10-cm needle-to-foil distance, and a 0.1 mL/h volumetric flow rate.

In an attempt to increase the solubility, side chains with various structures were used to determine the effects of the size/length, π bonds, and hydrogen bonds on the solubility and morphology of the resulting fibers. To aid in the selection of side groups and solvents, the theoretical solubilities were considered. The solubility parameter for each functionalized ANF type was estimated[24,25] and compared to those of the solvents,[26] as reported in Table I. The solubility parameter of each functionalized polymer (δ_i) was calculated as follows:

$$\delta_i = \frac{\sum F_i}{\hat{V}}$$

where F_i is the molar attraction constant of the polymeric moieties ($cal^{1/2}$ $mL^{1/2}$) and $\hat{V}$ is the polymer molar volume (mL/mol). For adequate solubility, the difference in the solubility parameters between the polymer and solvent should typically be less than 0.5 $MPa^{1/2}$.[24] However, factors including the temperature, side-chain size, and polarity can cause that threshold to vary.

In practice, some discrepancies were observed between the expected and realized solubilities. The calculated solubility parameters suggested a preferred solubility for propyl, allyl,

Table II. Dependence of the Fiber Diameter on the Electrospinning Solution Concentration as Demonstrated by Propyl-Functionalized ANFs Dispersed in DMF at Various Polymer Concentrations

Propyl ANF concentration (wt % in DMF)	Fiber diameter (nm)
20	67.2 ± 21.5
30	149 ± 65.1
35	309 ± 75.8
40	525 ± 121
50	1750 ± 377

The electrospinning conditions were 0.1 mL/h, a voltage of 20 kV, and a spinning distance of 10 cm.

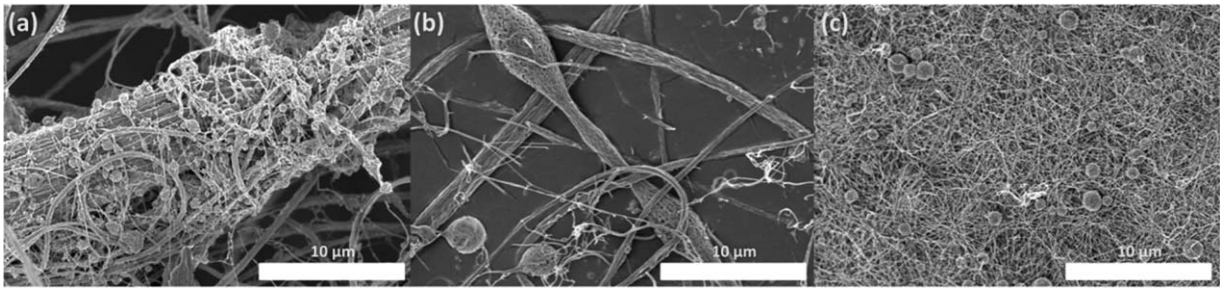

Figure 4. Attempts to electrospin propyl ANFs from DMF solutions with various operating parameters: (a) 20 wt % at 10 kV and 0.05 mL/h, (b) 20 wt % at 10 kV and 0.1 mL/h, and (c) 20 wt % at 20 kV and 0.05 mL/h. This illustrates fiber necking and beading under nonoptimal conditions.

pentenyl, and hydroxypropyl ANFs in the DMAc and NMP solvents. Allyl-, propyl-, and pentenyl-functionalized fibers were all soluble in DMF, DMAc, and NMP. Methyl and benzyl ANFs were expected to be generally insoluble in all three spinning solvents, yet were successfully dispersed and electrospun in NMP only or DMAc and NMP, respectively. Benzyl side chains demonstrated solubility in only DMAc or NMP as the solvent, whereas methyl-functionalized fibers required a higher boiling point NMP for solvation. These unexpected insolubilities were likely due to effects in hydrogen bonding, polarity and functional group size that were not captured by the calculations. Fibers functionalized with hydroxypropyl immediately precipitated out of DMSO and could not be redissolved in any organic solvent. The hydroxypropyl ANFs were generally insoluble; this was attributed to the additional hydrogen bonding, which was unaccounted for in the molar attraction values. Despite the lack of a strict correlation between the calculated and observed solubilities, these calculations provided guidance on side-chain/solvent combinations to pursue. To better understand the polymer solubility dynamics and control the resulting fiber morphology and crystalline properties, different functional groups, degrees of functionalization, and combinations of functional groups will be investigated in the future. Every side-chain/solvent combination that resulted in ANF solubility was further investigated for applicability in electrospinning.

Functionalized ANF dispersions were next vacuum-distilled and dispersed to concentrations up to 50 wt % in organic solvents suitable for electrospinning (i.e., DMF, DMAc, and/or NMP). Functionalized ANFs before electrospinning (Figure 2) were comparable in size to unfunctionalized fibers that were similarly dried from DMSO dispersions [Figure 1(b)]. Furthermore, electrospun functionalized ANFs (Figure 3) were significantly larger in diameter than the fibers seen in the parent spinning solution (Figure 2). This suggested that single electrospun fibers were composed of multiple ANFs of smaller diameter.

Electrospinning

The flow rate, voltage, solution concentration, and collector distance were varied to determine conditions sufficient for continuous electrospinning. Polymer concentrations in the range 20–50 wt % yielded nanofibers, with the fiber diameter increasing with spinning solution concentration (see Figure 3 and Table II). Relatively low volumetric flow rates (0.1 mL/h) were required along with a high electric field (20 kV at a 10-cm distance) to consistently obtain functionalized ANFs with a high uniformity. Higher volumetric flow rates and lower applied voltages resulted in the electrospraying of the polymer solution (i.e., polymer beading) and no fiber formation (Figure 4).

ANF Chemical and Structural Characterization

^{13}C ssNMR was conducted to provide insight into the molecular structure of the functionalized ANFs and to confirm proper substitution of the side groups onto the polymer chain. Analyses of methyl-, propyl-, and benzyl-functionalized ANFs are shown in Figure 5. Figure 5(a) shows the ^{13}C ssNMR spectra

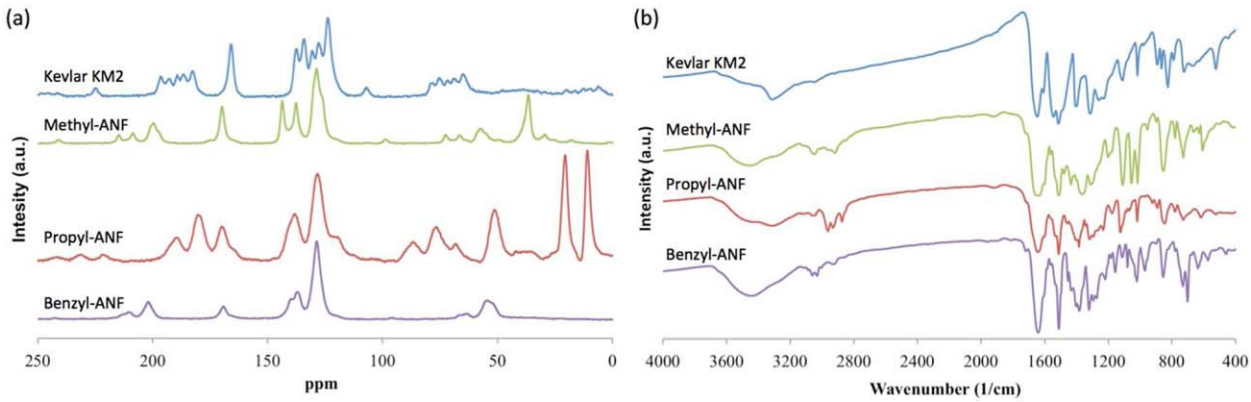

Figure 5. (a) ^{13}C ssNMR spectra and (b) transmission FTIR spectra for Kevlar KM2 and methyl, propyl, and benzyl ANFs. [Color figure can be viewed in the online issue, which is available at wileyonlinelibrary.com.]

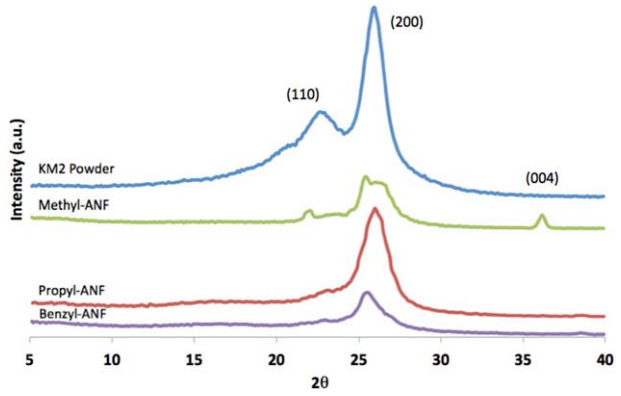

Figure 6. XRD spectra for Kevlar KM2 (in powder form) and functionalized ANFs, with methyl ANFs demonstrating reflectance peaks for (110) and (004) in addition to the ubiquitous (200) peak attributable to the maintained long-chain ordering. [Color figure can be viewed in the online issue, which is available at wileyonlinelibrary.com.]

for the three functionalized ANFs and Kevlar KM2. The spectrum for the benzyl-functionalized ANFs revealed an additional aliphatic carbon, as indicated by the shoulder of the peak at 50 ppm, which was not present in the spectrum of Kevlar. The additional aromatic carbons were obscured in the region from 120 to 150 ppm. The methyl functionalization was confirmed by the presence of a single aliphatic carbon peak at 45 ppm in the ssNMR spectrum. The spectrum for propyl-functionalized ANFs revealed three aliphatic carbons present in the propyl ANF sample that were not seen in the ssNMR of Kevlar, as indicated by the three broad peaks at 50, 20, and 10 ppm. The presence of C—H stretching peaks (3000–2800 cm^{-1}) in the FTIR spectra [Figure 5(b)] was indicative of the presence of alkyl C—H bonds in each of the three functionalized ANFs; this was associated with a decrease in the N—H stretching intensity (3325 cm^{-1}) relative to the Kevlar KM2 spectrum. The remaining presence of an N—H stretching peak in the functionalized ANF spectra was consistent with the findings from elemental analyses, which showed 71.3 ± 0.2% of ANF amides were alkylated. These data confirmed that functionalization reactions were occurring as expected.

XRD was used to investigate variations in the resulting fiber crystallinity as a function of side-group functionalization and spinning conditions. The XRD spectra of the electrospun methyl-, propyl-, and benzyl-functionalized ANFs and Kevlar KM2 (in powder form) are shown as examples in Figure 6. The XRD spectrum for Kevlar KM2 revealed a monoclinic crystal structure, including (110) and (200) reflectance peaks.[13,27] The methyl ANFs (spun from NMP) demonstrated (110), (200), and (004) reflection peaks, whereas only (200) peaks were identifiable for the propyl and benzyl ANFs (spun from DMF and DMAc, respectively). The presence of primarily only (200) reflections for all of the ANFs was indicative of a maintained

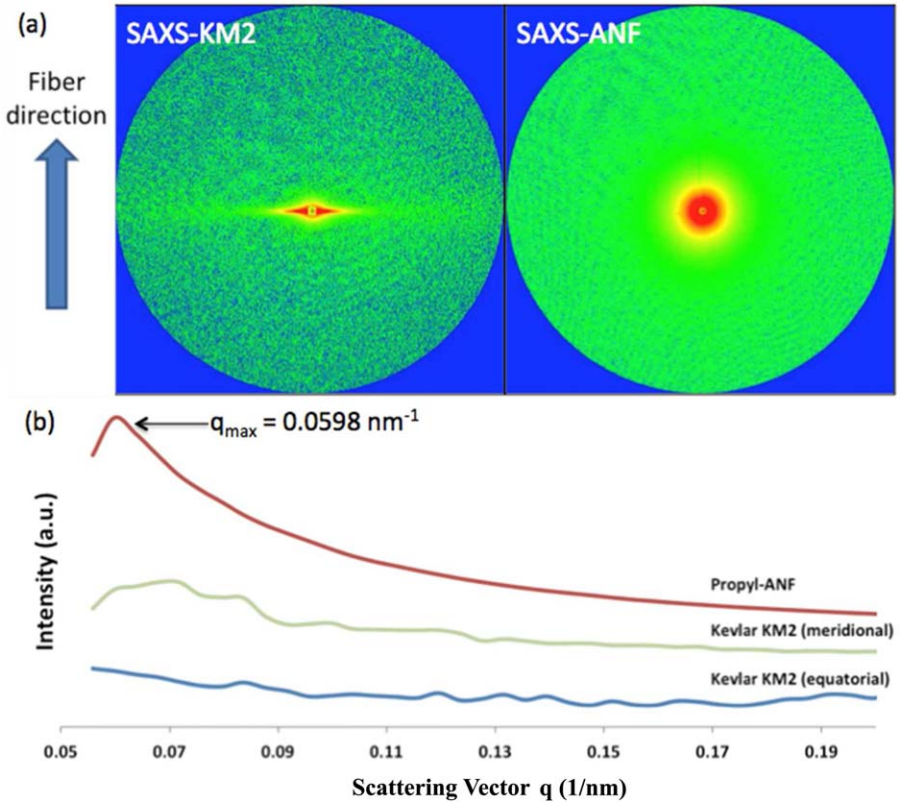

Figure 7. (a) 2D SAXS spectra for Kevlar KM2 fibers (left) and propyl ANFs (right) with the indicated fiber direction and (b) integrated 1D spectra for the propyl ANF and the Kevlar KM2 fiber along the equatorial and meridional directions. A q_{max} (first maximum of the scattering vector) value of 0.0598 nm^{-1} was equated to a long period of 105 nm for the propyl ANF, whereas numerous spectral maxima were observed for the Kevlar KM2 with an associated long period of 87 nm. [Color figure can be viewed in the online issue, which is available at wiley onlinelibrary.com.]

long-chain order in the crystalline regions, but without clear chain orientation, as evidenced by the absence or diminishment of other peaks (i.e., a disruption in the transverse periodicity, which was most likely due to the bulkier side chain moieties). These crystallographic changes very likely altered the material properties of these polymers, and methods for the nanoscale mechanical evaluation of these nanofibers will be the focus of future research efforts.

To determine the fiber morphologies on the order of a few to several hundred nanometers, SAXS was performed on both the as-received Kevlar KM2 and propyl ANFs (spun from DMF). The 2D SAXS patterns and 1D-integrated SAXS spectra are shown in Figure 7. The SAXS spectra for the Kevlar control sample showed a strong equatorial diffraction streak [Figure 7(a)] that has been observed in many synthetic fibers[28] and was indicative of a microfibrillar superstructure containing microvoids,[29] which are generally present in the amorphous region of the fiber. Conversely, the treated ANFs did not demonstrate any void scattering along the equatorial region; this indicated a loss in both the oriented fibrillar and microvoid morphologies because of the effects of *N*-substitution. This loss of fibrillar orientation was consistent with the presence of only (200) XRD reflections in the propyl ANFs. Furthermore, the fiber long period was calculated with the first maximum of the scattering vector (q_{max}):

$$\text{Long period} = (2\pi)/q_{max}$$

This gave a value of 105 nm ($q_{max} = 0.0598\ \text{nm}^{-1}$) for the propyl ANFs. The as-received Kevlar KM2 exhibited a long period of 87 nm, a value consistent with literature and unique to the defect band structure of aramids.[27,30–32] This greater long period for propyl ANFs suggested an increase in the overall size of the amorphous region of the fibers.

In combination with the XRD results listed previously, these SAXS findings suggested that the functionalized ANFs were comprised of long-chain, nonoriented crystalline domains separated by larger amorphous regions, which lacked the microvoid defects observed in commercial Kevlar. The microvoids present in commercial Kevlar are known to be an unavoidable result of the coagulation bath step of the dry wet-jet spinning method.[33] Conversely, the electrospinning of the functionalized ANFs resulted in fibers with amorphous regions that did not contain undesirable microvoids; this was likely due to the rapid solvent evaporation that occurred during the electrospinning process. The means to further tune the crystallite sizes and orientation by tailoring side-chain moieties and electrospinning conditions offer the potential to optimize the structures of these nanofibers and will potentially lead to virtually defect-free and highly crystalline and, therefore, high strength/high stiffness nanofibers. The influence of these structural optimizations on the physical and mechanical properties of the electrospun fibers will be the focus for future research endeavors.

CONCLUSIONS

In this article, we have reported the first practical, scalable method for the production of uniformly sized nanoscale fibers of functionalized PPTA. This method was used to prepare various *N*-functionalized PPTA nanofibers, or ANFs, on a multigram scale. The ANF crystalline structure was analyzed via XRD and SAXS, which suggested that the functionalized ANFs consisted of nonoriented crystalline domains surrounded by large amorphous regions that lacked the microvoid defects seen in commercial Kevlar fibers. Further investigation into the influence of chemical side chains and the electrospinning conditions as they relate to the resulting mechanical properties of these fibers is ongoing to ensure that the high-performance characteristics and nature of microscale Kevlar is retained during the transformation of fibers to the nanoscale.

ACKNOWLEDGMENTS

The authors thank Dr. Mayer (State University of New York at Stony Brook) for performing SAXS at the Brookhaven National Laboratory. This material based up on work supported by the U.S. Special Operations Command under contract No. H92222-13-C-0028.

REFERENCES

1. Curgul, S.; Vliet, K. J. V.; Rutledge, G. C. *Macromolecules* **2007**, *40*, 8483.
2. Baji, A.; Mai, Y.-W.; Wong, S.-C.; Abtahi, A. M.; Chen, P. *Compos. Sci. Technol.* **2010**, *70*, 703.
3. Deitzel, J. M.; Kleinmeter, J.; Harris, D.; Tan, N. C. B. *Polymer* **2001**, *42*, 261.
4. Li, D.; Xia, Y. *Adv. Mater.* **2004**, *16*, 1151.
5. Gibson, P. W.; Gibson, H. L.; Rivin, D. *AIChE J.* **1999**, *45*, 190.
6. Kim, J. S.; Reneker, D. H. *Polym. Compos.* **1999**, *20*, 124.
7. Papkov, D.; Zou, Y.; Andalib, M. N.; Goponenko, A.; Cheng, S. Z. D.; Czenis, Y. A. *ACS Nano* **2013**, *7*, 3324.
8. Huang, Z.-M.; Zhang, Y.-Z.; Kotaki, M.; Ramakrishna, S. *Compos. Sci. Technol.* **2003**, *63*, 2223.
9. Subbiah, T.; Bhat, G. S.; Tock, R. W.; Parameswaran, S.; Ramkumar, S. S. *J. Appl. Polym. Sci.* **2005**, *96*, 557.
10. Srinivasan, G.; Reneker, D. H. *Polym. Int.* **1995**, *36*, 195.
11. Hogg, P. *J. Science* **2006**, *314*, 1100.
12. Tanner, D.; Fitzgerald, J. A.; Phillips, B. R. *Angew. Chem. Int. Ed. Engl.* **1989**, *28*, 649.
13. Chatzi, E. G.; Koenig, J. L. *Polym.–Plast. Technol. Eng.* **1987**, *26*, 229.
14. Jassal, M.; Ghosh, S. *Indian J. Fibre Text.* **2002**, *27*, 290.
15. Yang, M.; Cao, K.; Sui, L.; Qi, Y.; Zhu, J.; Waas, A.; Arruda, E. M.; Kieffer, J.; Thouless, M. D.; Kotov, N. A. *ACS Nano* **2011**, *9*, 6945.
16. Cao, K.; Siepermann, C. P.; Yang, M.; Waas, A. M.; Kotov, N. A.; Thouless, M. D.; Arruda, E. M. *Adv. Funct. Mater.* **2013**, *23*, 2072.
17. Takayanagi, M.; Ueta, S.; Lei, W.-Y.; Koga, K. *Polym. J.* **1987**, *19*, 467.
18. Takayanagi, M.; Katayose, T. *J. Polym. Sci.* **1983**, *21*, 31.

19. Takayanagi, M.; Kajiyama, T.; Katayose, T. *J. Appl. Polym. Sci.* **1982**, *27*, 3903.
20. Takayanagi, M.; Katayose, T. *J. Polym. Sci.* **1981**, *19*, 1133.
21. Ai, T.; Wang, R.; Zhou, W. *Polym. Compos.* **2007**, *28*, 412.
22. Rasband, W. ImageJ, version 1.42. National Institute of Health; http://rsbweb.nih.gov/ij/index.html (accessed July 2014).
23. Hotaling, NA. DiameterJ, version 1.013. National Institute of Standards and Technology; http://imagej.net/DiameterJ (accessed July 2014).
24. Small, P. A. *J. Appl. Chem.* **1953**, *3*, 71.
25. Koenhen, D. M.; Smolders, C. A. *J. Appl. Polym. Sci.* **1975**, *19*, 1163.
26. Aharoni, S. M. *J. Appl. Polym. Sci.* **1992**, *45*, 813.
27. Ahmed, D.; Hongpeng, Z.; Haijuan, K.; Jing, L.; Yu, M.; Muhuo, Y. *Mater. Res.* **2014**, *17*, 1180.
28. Hoogsteen, W.; Ten Brinke, G.; Pennings, A. J. *J. Mater. Sci.* **1996**, *25*, 1551.
29. Ran, S.; Fang, D.; Zong, X.; Hsiao, B.; Chu, B.; Cunniff, P. *Polymer* **2001**, *42*, 1601.
30. Panar, M.; Avakian, P.; Blume, R. C.; Gardner, K. H.; Gierke, T. D.; Yang, H. H. *J. Polym. Sci. Polym. Phys. Ed.* **1983**, *21*, 1955.
31. Morgan, R. J.; Pruneda, C. O.; Steele, W. J. *J. Polym. Sci. Polym. Phys. Ed.* **1983**, *21*, 1757.
32. Dobb, M. G.; Park, C. R.; Robson, R. M. *J. Mater. Sci.* **1992**, *27*, 3876.
33. Dobb, M. G.; Robson, R. *J. Mater. Sci.* **1990**, *25*, 459.